Article:

Yu, Y. X., Ma, C., Qi, Chong et al. (2026) Evolution and coexistence of low-lying configurations in the N=80 isotones. Physical Review C. 024332. ISSN: 2469-9993

https://doi.org/10.1103/d6vm-5jfl

Evolution and coexistence of low-lying configurations in the $N = 80$ isotones

Y. X. Yu,[1] C. Ma,[2] Chong Qi,[3] W. Q. Zhang,[4] Calvin W. Johnson,[5] Z. Liu,[4] A. N. Andreyev,[6] and G. J. Fu[1,*]

[1] *School of Physics Science and Engineering, Tongji University, Shanghai 200092, China*
[2] *School of Science, Yanshan University, Qinhuangdao 066004, China*
[3] *Department of Physics, KTH Royal Institute of Technology, 10691 Stockholm, Sweden*
[4] *Institute of Modern Physics, Chinese Academy of Sciences, Lanzhou 730000, China*
[5] *Department of Physics, San Diego State University, 5500 Campanile Drive, San Diego, CA 92182-1233*
[6] *School of Physics, Engineering and Technology, University of York, York, YO105DD, United Kingdom*

(Dated: July 9, 2026)

Background: The $N = 80$ isotones offer an important opportunity for studying nuclear structure evolution and the interplay between single-particle motion and collective behavior near the $N = 82$ shell closure. Although the nuclear shell model is a powerful and predictive framework, progress for the open-shell nuclei has been limited by the rapidly increasing configuration-space dimensions and the lack of a reliable effective interaction.

Purpose: To construct a feasible shell-model Hamiltonian capable of describing the $N = 80$ even-even isotonic chain with Z = 50-74, and to investigate their underlying low-lying configurations.

Methods: Full-configuration-interaction shell-model calculations are performed in a model space that includes the proton and neutron orbitals $0g_{7/2}$, $1d_{5/2}$, $1d_{3/2}$, $2s_{1/2}$, and $0h_{11/2}$. The effective interaction is derived by optimizing the monopole and multipole components of the realistic interactions, reducing the number of independent parameters to eight via the principal component analysis approach. Further analysis is carried out using the nucleon-pair approximation of the shell model.

Results: The calculation reproduces excitation energies and electromagnetic properties for known $N = 80$ isotones and provides predictions for ^{150}Yb, ^{152}Hf, and ^{154}W near the proton drip line, including a level inversion between the yrast 18^+ and 20^+ states in ^{154}W. It further reveals a systematic evolution of the low-lying structures with increasing proton number.

Conclusions: The $N = 80$ isotones exhibit coexistence of multiple configurations: the yrast 0^+-4^+ states are (generalized-)seniority-dominated for lower-Z nuclei, becoming increasingly vibrational-like with growing valence proton number, while the yrast 6^+-10^+ states undergo transitions among neutron seniority-2, proton seniority-2, and proton-neutron coupled configurations along the isotonic chain, driven by proton-neutron interactions and the evolution of the proton Fermi surface. The analysis of the predicted level inversion in ^{154}W highlights the essential role of the isoscalar spin-aligned proton-neutron correlation.

I. INTRODUCTION

A central challenge in nuclear physics is to understand how low-lying excitations and emerging collectivity evolve as nuclei move away from closed shells. In the region between the magic numbers 50 and 82, where both valence protons and neutrons occupy the same major shell, extensive experimental and theoretical studies have been carried out to probe such evolution [1–14]. The interplay between single-particle and collective degrees of freedom in this region, involving proton and neutron g_7dsh_{11} orbitals ($0g_{7/2}$, $1d_{5/2}$, $1d_{3/2}$, $2s_{1/2}$, $0h_{11/2}$), serves as an essential mechanism for the transition from seniority-type structure in semi-magic nuclei to collective motions in open-shell nuclei.

In particular, experimental investigations of very neutron-deficient nuclei near the $N = 82$ shell closure have advanced considerably. Recent achievements include the high-precision mass measurement of $^{151}_{70}$Yb$_{81}$ [15], the first spectroscopy of $^{150}_{70}$Yb$_{80}$ [16], and the discovery of a new isotope $^{156}_{74}$W$_{82}$ [17, 18]. These studies, together with measurements of lifetimes, electromagnetic properties, and level schemes in neighboring nuclei, have revealed nuclear structure evolution as the proton number increases beyond the $Z = 64$ subshell closure. They also confirm the robustness of the $N = 82$ shell closure near or beyond the proton drip line [15–17]. Reliable theoretical studies are important to interpret the observed phenomena and to provide guidance for further experimental studies.

Among various theoretical approaches, the full-configuration-interaction shell model (SM) remains one of the most powerful tools for describing the struc-

*Electronic address: gjfu@tongji.edu.cn

ture and decay properties of nuclei [19–23]. Systematic SM calculations have been successful for the semi-magic $N = 82$ isotones [24–28]. However, progress for the open-shell isotones with $N < 82$ was limited, owing to the rapidly increasing dimensions of the configuration space and the lack of an accurate effective interaction applicable across a wide range of nuclei in this region. For the $N = 81$ odd-mass isotones, previous works include the SM studies of $^{133}_{52}$Te, $^{135}_{54}$Xe, and $^{137}_{56}$Ba [29], the phonon-model calculations for ^{133}Te-^{141}Nd [30], and systematic Hartree-Fock-Bogoliubov calculations of yrast $3/2^+$, $1/2^+$, and $11/2^-$ states in ^{133}Te-^{151}Yb [15, 31]. For the $N = 80$ even-even isotones, the large-scale SM [32] and the sampling-truncation calculations [33] have been carried out for ^{132}Te-^{140}Nd. The nucleon-pair approximation of the SM [34, 35] extends to ^{142}Sm, but does not go beyond the $Z = 64$ subshell closure.

In the present work, we perform large-scale SM calculations for the $N = 80$ even-even isotonic chain with Z = 50-74, optimizing the effective interaction using the principal component analysis (PCA) approach [36–38]. We systematically investigate low-lying even-parity states, electric quadrupole transition probabilities, and magnetic dipole moments. Good agreement with experimental data is achieved. We further analyze the underlying structural transitions of the low-lying states and predict the properties of the very neutron-deficient isotones ^{150}Yb, ^{152}Hf, and ^{154}W.

The paper is organized as follows. Sec. II briefly introduces the model space and the PCA optimization procedure for the effective interaction. Sec. III presents the calculation results, including electromagnetic properties, single-particle states in $N = 81$ odd-mass isotones, low-lying spectra in the $N = 80$ isotones, and a predicted level-inversion phenomenon in ^{154}W. Finally, Sec. IV summarizes the results.

II. THEORETICAL FRAMEWORK

For the $N = 80$ isotonic chain, we consider both valence protons and valence neutrons in the g_7dsh_{11} shell, including the $0g_{7/2}$, $1d_{5/2}$, $1d_{3/2}$, $2s_{1/2}$, and $0h_{11/2}$ orbitals, taking the doubly magic nucleus ^{100}Sn ($N = Z = 50$) as an inert core. The large-scale SM calculations are performed using the BIGSTICK code [39, 40]. The largest dimension encountered in this work exceeds 7×10^9 for the even-parity states with total magnetic quantum number $M = 0$ in ^{146}Dy. The significantly unbalanced numbers between the valence protons and the valence neutron holes result in a highly asymmetric many-body basis, leading to substantial challenges for large-scale parallel SM solvers using on-the-fly Hamiltonian reconstruction [39] such as BIGSTICK.

The SM Hamiltonian consists of proton and neutron single-particle energies (SPEs), as well as proton-proton, neutron-neutron, and proton-neutron two-body interactions. The proton SPEs and the proton-proton interaction are adopted from the monopole- and multipole-optimized effective interaction introduced in Refs. [27, 41], which well reproduces low-lying structures in the $N = 82$ isotones. This interaction was constructed from the realistic JJ56PNA interaction [42], with all proton-proton two-body matrix elements scaled by a factor of 0.82 and further optimized by refining the monopole component, the multipole components of ranks 2, 3, and 5, and the octupole-pairing force. The proton SPEs were originally determined for calculations with a ^{132}Sn core. To obtain the proton SPEs appropriate for the framework based on the ^{100}Sn core, we apply the Pandya transformation [19, 43]. The neutron SPEs and the neutron-neutron interaction are taken from a monopole-optimized Hamiltonian based on the realistic CD-Bonn potential, which successfully describes low-lying states in the Sn isotopes [10]. The excitation energies of the yrast $7/2^+$, $5/2^+$, $3/2^+$, $1/2^+$, and $11/2^-$ states in ^{133}Sb and ^{131}Sn have been calculated. The results are consistent with the experimental data, as the proton and neutron SPEs are primarily based on measured excitation energies. The calculation predicts an $11/2^-$ ground state in ^{131}Sn lying 15 keV below the $3/2^+$ state, whose excitation energy has not yet been determined experimentally.

The proton-neutron interaction is empirically optimized in this work, also starting from the realistic CD-Bonn potential used in Ref. [10]. The optimization is achieved by introducing 14 correction terms that include monopole and multipole interactions. The corresponding correction coefficients are denoted by a_i (i = 1-14). Among them, 9 isoscalar $T = 0$ monopole corrections between the $0g_{7/2}$, $1d_{5/2}$, $0h_{11/2}$ orbitals and the $1d_{3/2}$, $2s_{1/2}$, $0h_{11/2}$ orbitals of the other nucleon type are introduced. In addition, 4 quadrupole-quadrupole terms are added for different orbital couplings, such as those involving the proton and neutron $0h_{11/2}$ orbitals, the $1d_{3/2}$, $2s_{1/2}$ orbitals coupled with $1d_{3/2}$, $2s_{1/2}$, $0h_{11/2}$ orbitals of the other nucleon type, the $0g_{7/2}$, $1d_{5/2}$ orbitals coupled with $0g_{7/2}$, $1d_{5/2}$, $1d_{3/2}$, $2s_{1/2}$ orbitals of the other nucleon type, and the remaining orbital combinations. Finally, an isoscalar proton-neutron pairing term with $J = 11$ is considered.

The coefficients $\vec{a}$ [i)] are optimized through a least-

i) For convenience, we denote the 14 coefficients a_i collectively by the vector $\vec{a}$.

squares fit, combined with a PCA method [36–38] to reduce the dimension of the parameter space. The fitting procedure is as follows. Let N denote the total number of experimental data points used in the fit. The experimental value of the k-th data point is denoted by y^k, and the corresponding SM result by $f^k = f(k;\vec{a})$. Assuming the parameters are $\vec{a}^{(s)}$ at the s-th iteration, the gradient $\vec{g}^{k(s)}$ is defined by

$$g_i^{k(s)} \equiv \left.\frac{\partial f^k}{\partial a_i}\right|_{\vec{a}^{(s)}}. \tag{1}$$

The standard least-squares solution is obtained by solving the linear equations

$$A\Delta\vec{a} = \vec{b}, \tag{2}$$

where

$$A_{ij} = \sum_{k=1}^{N} g_i^{k(s)} g_j^{k(s)}, \tag{3}$$

$$\vec{b} = \sum_{k=1}^{N} (y^k - f^{k(s)})\vec{g}^{k(s)}. \tag{4}$$

Here $\Delta\vec{a}$ represents the parameter correction at the new iteration. To implement the PCA, the error matrix $D = A^{-1}$ is diagonalized as

$$\mathrm{diag}(d_1, d_2, \ldots, d_{14}) = PDP^T, \tag{5}$$

where the eigenvalues d_i are arranged in ascending order. The parameters $\vec{a}$ are then updated using

$$\vec{a}^{(s+1)} = \vec{a}^{(s)} + P^T \Delta\vec{c}', \tag{6}$$

with

$$\Delta c'_i = \begin{cases} d_i e_i, & \text{if } \; i \leqslant q, \\ 0, & \text{otherwise}, \end{cases} \tag{7}$$

where $\vec{e} \equiv P\vec{b}$, and q defines the dimension of the truncated parameter space, i.e., the number of retained principal parameters. The above steps are iterated until convergence is reached. Further details of the procedure are provided in Ref. [28]. Similar parameter-space truncation techniques have been widely used in optimizations of SM two-body matrix elements [44–50].

In this work, we truncate the parameter space to $q = 8$, meaning that the 14 correction terms are effectively combined to only eight independent degrees of freedom. The PCA-based optimization is performed using 73 experimental data points of excitation energies, including 55 data for selected yrast and yrare 0^+, 2^+, 4^+, 6^+, 8^+, and 10^+ states in the $N = 80$ even-even nuclei with $Z = 52$-$62, 68$ [51–57], one data point for the yrast 8^+-10^+ level spacing in ^{150}Yb [16], and 17 data for the yrast $1/2^+$, $3/2^+$, and $11/2^-$ states in $N = 81$ odd-mass nuclei with $Z = 52$-$64, 68, 70$ [15, 58–65]. The data for $^{144}_{64}$Gd and $^{146,147}_{66}$Dy are excluded from the fit to reduce computational cost due to their large configuration-space dimensions, and the 0^+-6^+ states of ^{150}Yb are excluded and left as predictions.

III. RESULTS AND DISCUSSION

In this section, we present our calculation results and analyze the nuclear structure of the $N = 80$ isotones.

A. Calculations of electromagnetic properties

The reduced electric-quadrupole transition strength $B(E2)$ is defined as

$$B(E2;J_i \to J_f) \equiv \frac{1}{2J_i+1}\left| e_\pi \left\langle J_f \left\| \hat{Q}_{2\pi} \right\| J_i \right\rangle + e_\nu \left\langle J_f \left\| \hat{Q}_{2\nu} \right\| J_i \right\rangle \right|^2, \tag{8}$$

where e_π and e_ν denote the proton and neutron effective charges, and the quadrupole operator $\hat{Q}_2$ is defined as

$$\hat{Q}_2 = \hat{r}^2 \hat{Y}_2. \tag{9}$$

$\langle J_f || \hat{Q}_2 || J_i \rangle$ represents the reduced matrix element in the Edmonds convention.

Fig. 1(a) provides a global comparison of $B(E2)$ transition strengths in the $N = 80$ isotones between the SM results and 26 experimental values listed in Table I in the Appendix. When using effective charges $e_\pi = 1.5e$ and $e_\nu = 1.1e$, most points align along the diagonal in the figure, indicating overall agreement with experiment. In contrast, the calculation with the standard effective charges $e_\pi = 1.5e$ and $e_\nu = 0.5e$ show relatively larger deviations from the data. Previous SM studies have similarly suggested that a neutron effective charge larger than $0.8e$ is required in reproducing the $B(E2)$ transition strengths in Sn and Te isotopes as well as in several $N = 81$ odd-mass nuclei [10, 11, 29], while the standard proton effective charge is good to reproduce the $B(E2)$ transition strengths in $N = 82$ isotones [28].

There are, however, seven data points for which the SM result noticeably deviates from experiment. Three of them, marked as group A in Fig. 1(a), correspond to the $2_2^+ \to 0_1^+$ transitions in ^{134}Xe, ^{136}Ba, and ^{138}Ce, where the experimental $B(E2)$ values are 0.74(5) W.u., 0.89(25) W.u., and 1.15(4) W.u., respectively, while the calculated values are 3.05 W.u., 5.28 W.u., and 5.66 W.u. The fourth point, marked as B, corresponds to the $6_1^+ \to 4_2^+$

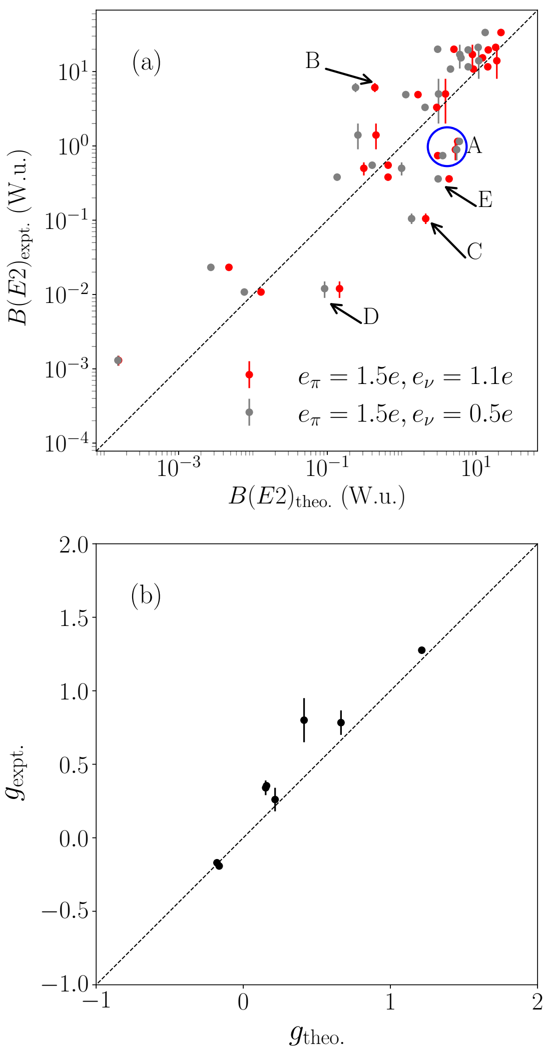

FIG. 1: (a) Comparison of experimental [16, 51–57, 66–69] and SM $B(E2)$ values for the $N = 80$ isotones. The dotted line denotes the equivalence of calculation and experiment. Seven data points deviate noticeably from this line: three points marked as group A correspond to the $2^+_2 \to 0^+_1$ transitions in ^{134}Xe, ^{136}Ba, and ^{138}Ce; the point marked as B corresponds to the $6^+_1 \to 4^+_2$ transition in ^{138}Ce; the point marked as C corresponds to the $6^+_1 \to 4^+_1$ transition in ^{138}Ce; and the points marked as D and E correspond to the $10^+_1 \to 8^+_1$ transitions in ^{148}Er and ^{150}Yb, respectively. (b) Comparison of experimental [52–55, 58, 67] and calculated g-factors for the $N = 80$ isotones.

transition in ^{138}Ce, for which the experimental value of $B(E2) = 6.1^{+0.9}_{-0.8}$ W.u. is much larger than the calculated value of 0.44 W.u. The fifth point, marked as C, corresponds to the $6^+_1 \to 4^+_1$ transition in the same nucleus, where the experimental value $B(E2) = 0.105^{+0.018}_{-0.016}$ W.u. is smaller than the calculated value of 2.10 W.u. Two additional points, marked as D and E, correspond to the $10^+_1 \to 8^+_1$ transitions in ^{148}Er and ^{150}Yb. Although a fully quantitative explanation of these deviations is not yet available, we note the following phenomena that may be relevant. Groups A and B involve inter-band $2^+_2 \to 0^+_1$ and $6^+_1 \to 4^+_2$ transitions, whose $B(E2)$ strengths are known to be difficult to reproduce accurately in shell-model calculations. For point C, the analysis presented in Sec. III D shows that the yrast 6^+_1 state in ^{138}Ce is dominated by the $6^+_\pi \otimes 0^+_\nu$ configuration, whereas the yrast 4^+_1 state is built mainly on the $2^+_\pi \otimes 2^+_\nu$ and $0^+_\pi \otimes 4^+_\nu$ configurations. The $E2$ operator cannot connect these major components, so the predicted $B(E2; 6^+_1 \to 4^+_1)$ strength is governed by minor components and is sensitive to the residual mixing in the wave functions. Finally, for points D and E, while the SM does not reproduce the absolute experimental $B(E2; 10^+_1 \to 8^+_1)$ values accurately, it does correctly reproduce the ratio: the $B(E2; 10^+_1 \to 8^+_1)$ transition probability in ^{150}Yb is about 30 times larger than that in ^{148}Er, which accounts for the much shorter experimental half-life of the 10^+_1 state in ^{150}Yb compared with the corresponding state in ^{148}Er [16, 69]. The experimental $B(E2; 10^+_1 \to 8^+_1)$ values are 0.012(3) W.u. for ^{148}Er and 0.36(3) W.u. for ^{150}Yb, respectively. The SM values are approximately one order of magnitude larger, which are 0.15 W.u. and 4.34 W.u., respectively.

The g-factor (alternatively, the magnetic dipole moment μ) is calculated by

$$g \equiv \frac{\mu}{J\mu_{\mathrm{N}}} \equiv \frac{1}{J} \times \langle J; M = J|\, g_{l\mathrm{p}}\hat{l}_{z\mathrm{p}} + g_{s\mathrm{p}}\hat{s}_{z\mathrm{p}} + g_{l\mathrm{n}}\hat{l}_{z\mathrm{n}} + g_{s\mathrm{n}}\hat{s}_{z\mathrm{n}}\, |J; M = J\rangle\,, \tag{10}$$

where we take the bare nucleon orbital g-factors and apply the standard quenching factor $g_s = 0.7$ to the nucleon spin g-factors, i.e., $g_{l\mathrm{p}} = 1.0$, $g_{l\mathrm{n}} = 0.0$, $g_{s\mathrm{p}} = 5.586g_s$, and $g_{s\mathrm{n}} = -3.826g_s$. Fig. 1(b) compares the calculated g-factors with 8 experimental values for the $N = 80$ isotones listed in Table II in the Appendix. The SM result is overall in good agreement with experiment, although a discrepancy is seen for the 4^+_1 state of ^{134}Xe, where the experimental value is 0.80(15), while the SM yields 0.41.

B. Single-neutron-hole states of $N = 81$ odd-mass nuclei

Before discussing the results for the $N = 80$ isotones in more detail, we examine the yrast $3/2^+$, $1/2^+$, and $11/2^-$ states in the $N = 81$ odd-mass isotones. These states are expected to be dominated by single-neutron-hole configurations, and their excitation energies are strongly influenced by the neutron SPEs and the proton-neutron monopole interactions, which together produce the spherical nuclear mean field. Fig. 2(a) shows the evolution of

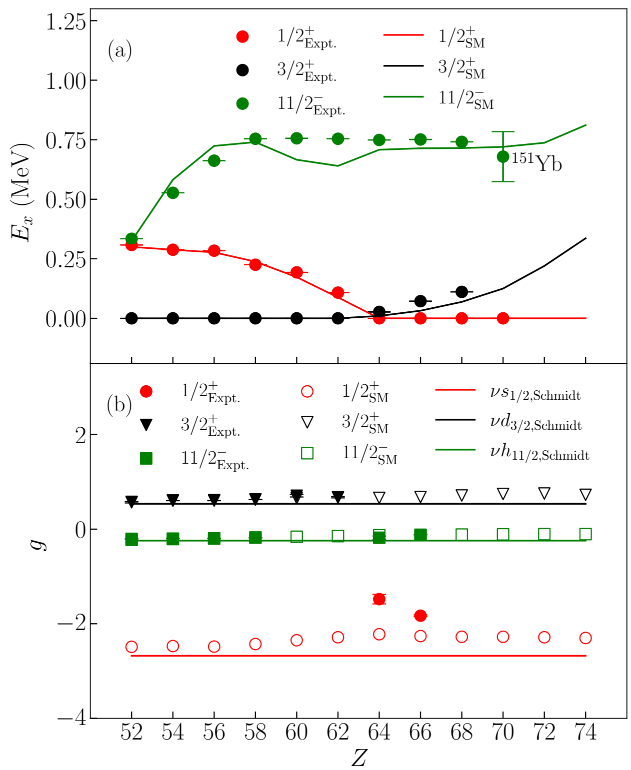

FIG. 2: (a) The excitation energies E_x and (b) the g-factors of the lowest-energy $3/2^+$, $1/2^+$, and $11/2^-$ states in the $N=81$ odd-mass isotones ^{133}Te-^{155}W. The experimental data are taken from Refs. [15, 58–65, 70]. The horizontal lines in panel (b) indicate the Schmidt values.

the energy levels along the $N=81$ isotonic chain. Experimentally, the ground-state spin and parity are $3/2^+$ from $^{133}_{52}$Te to $^{143}_{62}$Sm, and change to $1/2^+$ from $^{145}_{64}$Gd to $^{151}_{70}$Yb. For nuclei with $Z \geq 64$, the excitation energy E_x of the $3/2^+$ state gradually increases. The excitation energy of the $11/2^-$ state rises rapidly from $^{133}_{52}$Te to $^{139}_{58}$Ce, and then remains nearly constant from $^{141}_{60}$Nd to $^{149}_{68}$Er. Our SM calculation reproduces well these systematic trends, indicating that the optimized effective interaction used in this work reliably describes the shell evolution near $N=80$.

A recent mass measurement reported $E_x(11/2^-_1, {}^{151}\mathrm{Yb}) = 679(105)$ keV, representing a decrease of ≈ 70 keV relative to ^{149}Er [15]. In contrast, our SM calculation does not show this decrease but instead maintains an approximately constant trend extending to ^{153}Hf, with a slightly upward shift predicted for ^{155}W. Further experimental investigations in this region would be interesting.

Fig. 2(b) compares the SM g-factors for the yrast $3/2^+$, $1/2^+$, and $11/2^-$ states with the available experimental data and the Schmidt values, which are given by

$$g_j = \begin{cases} g_l + \frac{g_s - g_l}{2j}, & \text{if } j = l + \frac{1}{2}, \\ g_l - \frac{g_s - g_l}{2(j+1)}, & \text{if } j = l - \frac{1}{2}. \end{cases} \tag{11}$$

The experimental, SM, and Schmidt g-factors for the $3/2^+$ and $11/2^-$ states are in good agreement, confirming their predominantly single-neutron-hole character. For the $1/2^+$ states, the SM calculation predicts a dominant $s_{1/2}$ single-neutron-hole character, consistent with the Schmidt value. The available experimental values for ^{145}Gd and ^{147}Dy, however, slightly deviate from the calculation, possibly because low-spin states are generally more susceptible to stronger configuration mixing.

C. Low-lying structures of $N=80$ even-even nuclei

We also calculate the yrast and yrare 0^+, 2^+, 4^+, 6^+, 8^+, and 10^+ states for the even-even isotones ^{130}Sn-^{154}W, see Fig. 3. Overall, the SM calculation provides a good description of the available experimental data. Notably, the recently observed level scheme of ^{150}Yb, including the new 10^+ isomer [16], is well reproduced.

We first discuss the behavior of the yrast 2^+ and 4^+ states. Fig. 4 presents the ratio $R_{4/2} \equiv E_x(4^+_1)/E_x(2^+_1)$, an indicator of nuclear collectivity: values below 2 correspond to seniority-like structures, ratios ≈ 2 are characteristic of vibrational motion, and ratios close to 3.33 are characteristic of collective rotation. As shown in the figure, the SM result follows the experimental trend. For ^{130}Sn, the ratio is the smallest, with experimental and theoretical values of 1.594 and 1.567, respectively, consistent with seniority (or more precisely generalized seniority [ii] [19, 71]) states. From ^{130}Sn to ^{136}Ba, $R_{4/2}$ gradually increases to 2.28, with increasing $B(E2; 2^+_1 \to 0^+_1)$ and $B(E2; 4^+_1 \to 2^+_1)$ strengths (see Table I), indicating a smooth enhancement of collectivity as the valence proton number increases. Beyond ^{136}Ba, the ratio stabilizes around 2.3, exhibiting vibrational-like character. The major components of the yrast 0^+, 2^+, and 4^+ state wave functions are analyzed in Sec. III D, where the 4^+ states are shown to exhibit stronger configuration mixing.

The yrast 6^+ states in the $N=80$ isotones with $Z>50$ are primarily determined by proton configurations inherited from the neighboring $N=82$ isotones. In those $N=82$ nuclei the 6^+ states are dominated by seniority-2 components, with the two unpaired protons in the $(0g_{7/2})^2$ and $0g_{7/2}1d_{5/2}$ configurations for the

[ii] Hereafter, "generalized" is omitted for brevity.

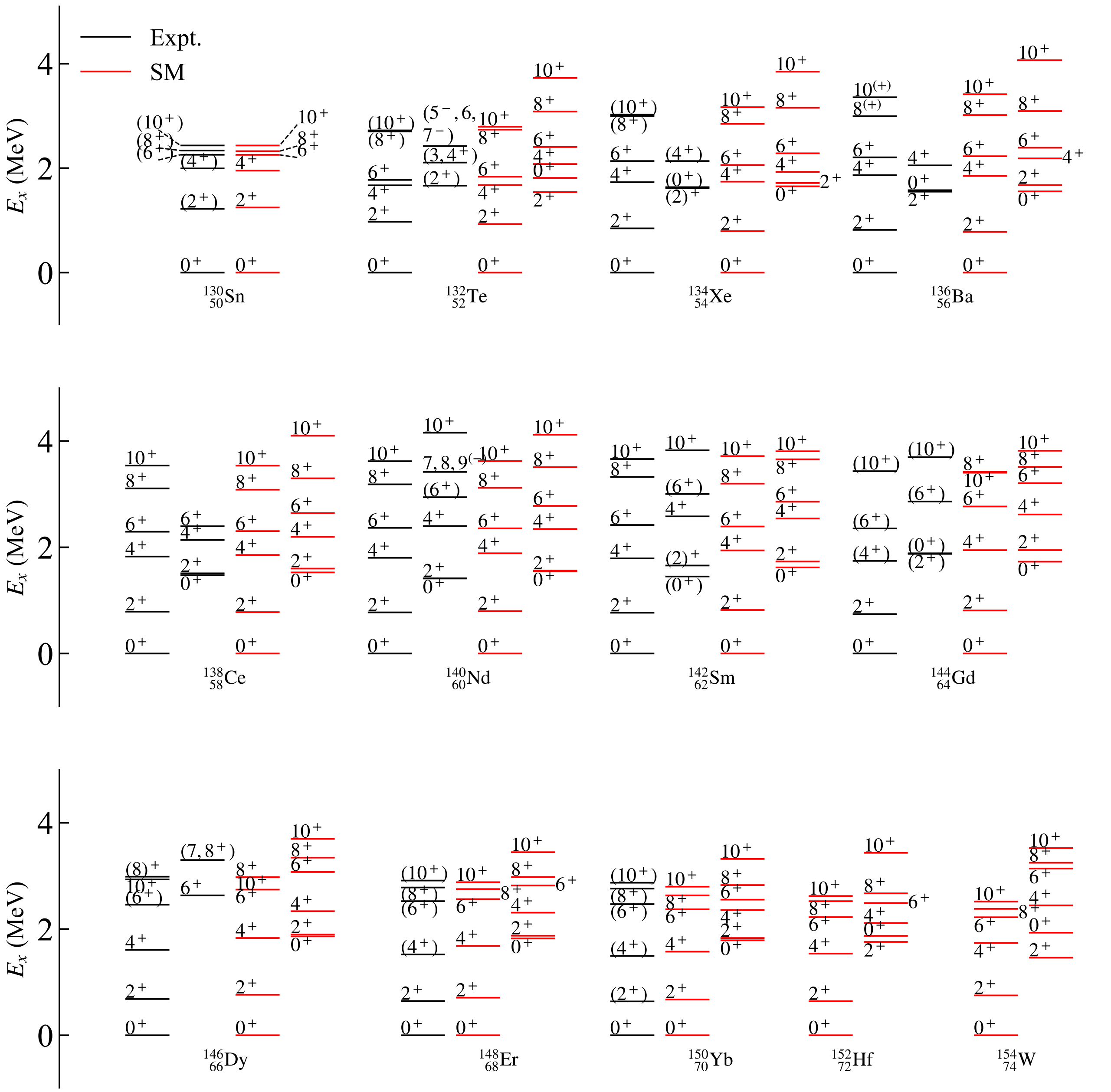

FIG. 3: The yrast and yrare 0^+, 2^+, 4^+, 6^+, 8^+, and 10^+ states in the $N = 80$ isotones ^{130}Sn-^{154}W. The black and red lines represent the experimental and SM values, respectively. The experimental data are taken from Refs. [16, 51–57, 66–68]. No experimental data are available for ^{152}Hf and ^{154}W; only theoretical predictions are shown.

lower-Z isotones, and in the $(0h_{11/2})^2$ configuration for the higher-Z isotones [28]. The correspondence between $N = 80$ and $N = 82$ is reflected in their g-factors: for instance, the experimental and SM g-factors of the 6^+ state in ^{132}Te are 0.783(83) and 0.664, respectively (see Table II), close to the SM value of 0.697 for ^{134}Te. As the 6^+ excitation energies in ^{132}Te and ^{134}Te differ by only about 80 keV, it is natural to suggest that the 6^+ state in ^{132}Te shares the same proton character as its $N = 82$ neighbor; we thus denote the dominant configuration as $6^+_\pi \otimes 0^+_\nu$. The analysis for these wave functions shown in Sec. III D confirms this assignment. For $Z = 54$-74, the SM g-factors of the 6^+ states (0.666-1.138) are close to those of the corresponding $N = 82$ isotones (0.694-

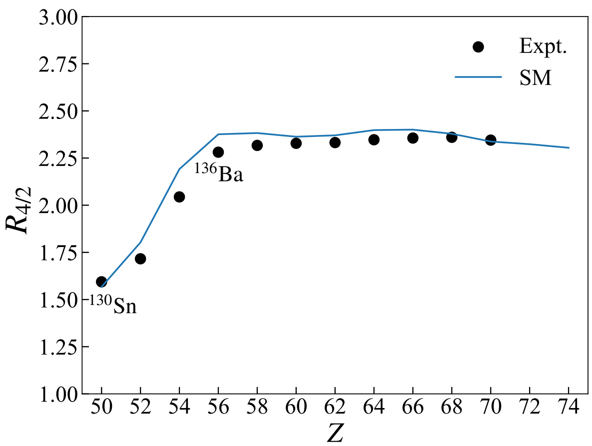

FIG. 4: The ratio of excitation energies, $R_{4/2} \equiv E_x(4_1^+)/E_x(2_1^+)$.

1.231), and their excitation energies exhibit similar systematic trends. For ^{130}Sn, the SM g-factor of the 6^+ state is -0.243, in good agreement with the Schmidt value of -0.244, consistent with the neutron-hole configuration $(0h_{11/2})_\nu^{-2}$.

Fig. 5(a) shows the g-factors of the 8^+ states along the $N = 80$ isotonic chain, which we have associated with the $(0h_{11/2})_\nu^{-2}$, $6_\pi^+ \otimes 2_\nu^+$, and $(0h_{11/2})_\pi^2$ configurations (the values are also listed in Table II in the Appendix). We find that the 8^+ state dominated by a particular configuration is yrast in some isotones and non-yrast in others, reflecting the evolution of the underlying structure. We therefore first discuss the yrast 8^+ states, which reveal a systematic transition in their dominant configurations, and then turn to the non-yrast 8^+ states later. For ^{130}Sn and ^{132}Te at lower Z, the SM 8_1^+ g-factors are -0.243 and -0.210, respectively, both close to the Schmidt value of -0.244 corresponding to the $(0h_{11/2})_\nu^{-2}$ configuration. At higher Z values, the SM g-factors of the yrast 8^+ states from ^{144}Gd to ^{154}W all exceed 1.15 (see Table II), close to the Schmidt value of 1.265, indicating that the $(0h_{11/2})_\pi^2$ configuration is dominant. For the intermediate region from ^{134}Xe to ^{142}Sm, the SM 8_1^+ g-factors range from 0.519 to 0.801, strongly deviating from the Schmidt values. Previous calculations within the nucleon-pair approximation of the SM suggest that these 8_1^+ states are dominated by proton-neutron coupled configurations $6_\pi^+ \otimes 2_\nu^+$ [35]. To interpret this pattern, we estimate the g-factors of such coupled states as [28, 72, 73]

$$g\left[(J_\pi \otimes J_\nu)^{(J)}\right] = \frac{J_\pi(J_\pi+1) - J_\nu(J_\nu+1)}{2J(J+1)}(g_{J_\pi} - g_{J_\nu}) + \frac{1}{2}(g_{J_\pi} + g_{J_\nu}). \tag{12}$$

Using $J_\pi = 6$, $J_\nu = 2$, and $J = 8$, we obtain

$$g\left[(6_\pi^+ \otimes 2_\nu^+)^{(8^+)}\right] = \frac{3}{4}g(6_\pi^+) + \frac{1}{4}g(2_\nu^+). \tag{13}$$

Here $g(6_\pi^+)$ is taken from our SM calculation for the corresponding $N = 82$ isotones, while $g(2_\nu^+)$ cannot be directly obtained[iii)]. However, for ^{134}Xe-^{142}Sm, our calculation shows that the neutron contributions to the SM 2_1^+ g-factors are 0.110-0.263, close to the total values of 0.152-0.260 (see Table II). This allows us to approximately evaluate $g(2_\nu^+)$ by these neutron components. Eq. (13) then yields $g\left[(6_\pi^+ \otimes 2_\nu^+)^{(8^+)}\right] = 0.548$-$0.836$, close to the SM results, supporting the configuration assignment suggested above. This demonstrates that the 8_1^+ states undergo a transition from neutron-dominated, through proton-neutron coupled, and to proton-dominated structures along the isotonic chain.

Interestingly, similar configuration patterns are found in the non-yrast 8^+ states. In ^{134}Xe-^{154}W, the SM calculation shows that the selected non-yrast 8^+ states are dominated by the $(0h_{11/2})_\nu^{-2}$ configuration. Their g-factors lie close to the neutron $h_{11/2}$ Schmidt value in ^{134}Xe-^{144}Gd, and deviate moderately from it in ^{146}Dy-^{154}W, with the largest deviation occurring in ^{148}Er (SM value of 0.322), reflecting considerable mixing with other configurations. In ^{136}Ba-^{142}Sm, the selected non-yrast 8^+ states have SM g-factors close to the proton $h_{11/2}$ Schmidt value, consistent with the $(0h_{11/2})_\pi^2$ configuration; the slightly lower g-factor in ^{136}Ba suggests relatively strong configuration mixing. Additionally, in ^{132}Te and ^{144}Gd-^{154}W, the selected non-yrast 8^+ states are consistent with the proton-neutron coupled $6_\pi^+ \otimes 2_\nu^+$ configurations, as their SM g-factors are close to those evaluated using Eq. (13).

The systematic trends of these 8^+ states, summarized in Fig. 6(a), can be understood in terms of the underlying shell structure. With increasing Z, the proton Fermi surface gradually approaches the $0h_{11/2}$ orbital, leading to a rapid decrease in the excitation energies of the proton-$(0h_{11/2})_\pi^2$-dominated 8^+ states. Simultaneously, the neu-

iii) The neutron part of the 8^+ wave function is strongly affected by the valence protons via the proton-neutron interaction, so the g-factor of ^{130}Sn 2^+ is not directly used as an estimator of $g(2_\nu^+)$ for the heavier isotones.

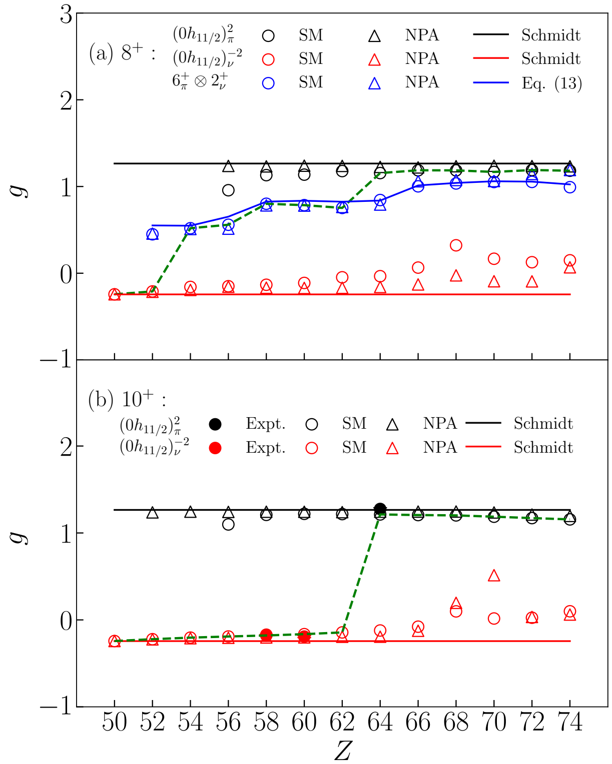

FIG. 5: g-factors of selected low-lying (a) 8^+ and (b) 10^+ states in the $N = 80$ isotones. Colors indicate the states dominated by different configurations: black for proton $(0h_{11/2})^{-2}_\pi$, red for neutron $(0h_{11/2})^{-2}_\nu$, and blue for proton-neutron coupled $6^+_\pi \otimes 2^+_\nu$ configurations. The open circles and triangles represent the SM and nucleon-pair approximation (NPA) calculations, respectively. The green dashed curves connect the g-factors for the yrast states. The solid lines in black and red show the $\pi h_{11/2}$ and $\nu h_{11/2}$ Schmidt g-values, respectively, and the blue curve indicates the g-values for the $6^+_\pi \otimes 2^+_\nu$ configuration estimated using Eq. (13). Note that no experimental data are available for the 8^+ states, and only three data points exist for the 10^+ states.

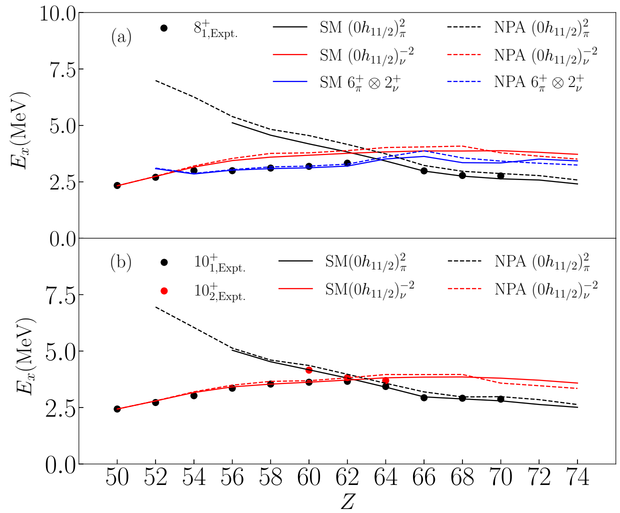

FIG. 6: Excitation energies of the low-lying (a) 8^+ and (b) 10^+ states in the $N = 80$ isotones. The solid points represent experimental data, the solid curves show the SM result, and the dotted curves correspond to the NPA calculation. Colors for the curves denote the states dominated by different configurations, as in Fig. 5. The figure illustrates the evolution of the low-lying 8^+ and 10^+ states and the good agreement between experiment, SM, and NPA.

tron $0h_{11/2}$ orbital is pushed down due to the proton-neutron monopole interaction [22, 74–78], which results in a gradual increase in the excitation energies of the neutron-hole-$(0h_{11/2})^{-2}_\nu$-dominated 8^+ states, also consistent with the trend of the $11/2^-$ levels observed in the neighboring $N = 81$ isotones. The excitation energies of the $6^+_\pi \otimes 2^+_\nu$-dominated 8^+ states remain relatively flat, similar to the 6^+_1 states. These combined behaviors produce the configuration coexistence and transition pattern along the $N = 80$ isotonic chain.

A similar analysis can be carried out for the 10^+ states along the $N = 80$ isotonic chain. The yrast 10^+ states are isomeric, as all measured half-lives exceed 10 ns [79], and they have attracted much experimental attention [69, 77, 80–86]. As shown in Fig. 5(b) and Fig. 6(b), the SM calculation predicts both neutron $(0h_{11/2})^{-2}_\nu$ and proton $(0h_{11/2})^2_\pi$ 10^+ states in the low-lying region. We note that experimental g-factors are available only for the yrast 10^+ states in three nuclei (^{138}Ce, ^{140}Nd, and ^{144}Gd), so most of the g-factor evidence comes from the SM predictions. The excitation energies of the $(0h_{11/2})^{-2}_\nu$ 10^+ states follow the trends of the $(0h_{11/2})^{-2}_\nu$ 8^+ states and the $11/2^-$ levels in the neighboring $N = 81$ isotones. The $(0h_{11/2})^2_\pi$ 10^+ states exhibit a similar downward trend as the $(0h_{11/2})^2_\pi$ 8^+ states, reflecting the evolution of the proton Fermi surface. These two 10^+ sequences cross in energy at $Z \approx 64$, such that the yrast 10^+ states from ^{130}Sn to ^{142}Sm are dominated by the $(0h_{11/2})^{-2}_\nu$ configuration, while those from ^{144}Gd to ^{154}W are predominantly $(0h_{11/2})^2_\pi$. The g-factors of the $(0h_{11/2})^{-2}_\nu$ 10^+ states behave like those of the 8^+ states: they stay close to the neutron $h_{11/2}$ Schmidt value over most of the isotonic chain, with a deviation for the isotones around ^{148}Er. The 10^+ configuration transition has been indicated in earlier works based on systematics [80, 81], although a consistent theoretical calculation has been lacking. A comprehensive discussion of this transition is presented in Ref. [16].

D. Analysis within the nucleon-pair approximation

To provide further microscopic insight into the SM interpretation of the low-lying 8^+ and 10^+ states in the $N = 80$ isotones, we use the nucleon-pair approximation (NPA) [87] to examine the wave function compositions and support the configuration assignments indicated by the SM g-factors. The NPA offers an efficient truncation of the SM configuration space by constructing many-body bases from collective nucleon pairs with specific angular momenta and parities,

$$\hat{A}^{(J)\dagger} \equiv \sum_{j_1 j_2} y_J(j_1 j_2) \left(\hat{a}^\dagger_{j_1} \times \hat{a}^\dagger_{j_2}\right)^{(J)}, \tag{14}$$

where $y_J(j_1 j_2)$ denotes the pair-structure coefficients determined through a variational principle [88–90]. Typical building blocks include the even-parity monopole S ($J = 0$) and quadrupole D ($J = 2$) pairs, as well as, if necessary, higher-J pairs like the G ($J = 4$), I ($J = 6$), K ($J = 8$), and M ($J = 10$) pairs. Energies and wave functions are obtained by diagonalizing the Hamiltonian in the space spanned by those nucleon-pair bases. The NPA basis is flexible: for example, if one considers the condensate of a collective S pair, it effectively corresponds to the generalized seniority scheme; if all possible nucleon pairs are included, the NPA configuration space is equivalent to the full SM. Unlike the interacting boson model, which maps collective pairs onto bosons, the NPA retains the underlying fermionic structure and uses SM interactions. This allows direct comparison with SM results while providing transparent microscopic interpretations of nuclear structure. The NPA has been shown to successfully describe properties in medium- and heavy-mass nuclei, demonstrating that only a few collective pair degrees of freedom dominate the low-lying states [91–93].

In this work, we calculate the $N = 80$ isotones within the NPA using the same SM Hamiltonian. For the valence protons, we include the S, D, G, I, K, and M pairs, restricting the number of $J > 2$ pairs to at most one. For the two valence neutron holes, we adopt the same set of pairs. The pair-structure coefficients $y_J(j_1 j_2)$ are obtained using the generalized seniority approach. The S pairs are determined by minimizing the energy of the seniority-0 state, i.e., the S-pair condensate,

$$\begin{aligned} \delta \frac{\langle \Psi(S^N) | \hat{H} | \Psi(S^N) \rangle}{\langle \Psi(S^N) | \Psi(S^N) \rangle} = 0, \\ |\Psi(S^N)\rangle \equiv \left(\hat{S}^\dagger_\pi\right)^{N_\pi} \left(\hat{S}^\dagger_\nu\right)^{N_\nu} |0\rangle, \end{aligned} \tag{15}$$

where N_π and N_ν are the numbers of valence proton pairs and valence neutron-hole pairs, and $N = N_\pi + N_\nu$. For the non-S pairs, we diagonalize the Hamiltonian in the subspace spanned by the seniority-2 states $\left(\hat{a}^\dagger_{j_1} \times \hat{a}^\dagger_{j_2}\right)^{(J)} |\Psi(S^{N-1})\rangle$, and take the expansion coefficients of the lowest eigenstate as the pair-structure coefficients. To account for the structural change from low-spin to high-spin states, we also consider a model space constructed from the pairs with modified pair-structure coefficients (see Ref. [35] for details). This NPA space is the same as that used in Ref. [35], which yielded excitation energies of the yrast states in ^{130}Sn-^{142}Sm in good agreement with both experiment and the SM result. Here, we extend the analysis to ^{154}W and to the non-yrast 8^+ and 10^+ states.

We first examine the yrast 0^+, 2^+, and 4^+ states. The 0^+ ground states are dominated by the seniority-0, namely $0^+_\pi \otimes 0^+_\nu$, configuration across the $N = 80$ chain, with contributions ranging from 65% to 90%. The yrast 2^+ states are dominated by the seniority-2 configuration $0^+_\pi \otimes 2^+_\nu$ (50–70%), while the $2^+_\pi \otimes 0^+_\nu$ configuration contributes 10–30% and the seniority-4 configuration $2^+_\pi \otimes 2^+_\nu$ contributes less than 10%. The yrast 4^+ states show more fragmented compositions that evolve with proton number Z. In ^{132}Te, the $4^+_\pi \otimes 0^+_\nu$ configuration dominates (64%), while the $2^+_\pi \otimes 2^+_\nu$ configuration contributes 26%. From ^{134}Xe to ^{152}Hf, the $2^+_\pi \otimes 2^+_\nu$ and $0^+_\pi \otimes 4^+_\nu$ configurations are the two leading components, contributing 30–45% and 15–40%, respectively, while the $4^+_\pi \otimes 0^+_\nu$ component becomes less important. In ^{154}W, the $4^+_\pi \otimes 0^+_\nu$ and $2^+_\pi \otimes 2^+_\nu$ configurations contribute 31% and 40%, respectively, while the $0^+_\pi \otimes 4^+_\nu$ configuration contributes only 11%. It is worth mentioning that the seniority states are highly correlated and are difficult to calculate in the shell-model m-scheme basis. The NPA, built on a pair basis, provides a well-developed framework for examining the seniority configuration structure of these states.

We next turn to the yrast 6^+ states. The NPA calculations show that the seniority-2 configuration $6^+_\pi \otimes 0^+_\nu$ is the leading component of the wave functions from ^{132}Te to ^{154}W, with contributions ranging from 40% to 75%. Moreover, the squared overlap between the proton part of this configuration in the $N = 80$ nuclei and the seniority-2 proton component of the yrast 6^+ states in the corresponding $N = 82$ isotones exceeds 94% for most isotones, confirming that the yrast 6^+ states in both chains share the same proton character.

The NPA calculation yields low-lying 8^+ and 10^+ states with excitation energies and g-factors in good agreement with the SM results, see Figs. 5 and 6. To more directly confirm the dominant configurations suggested by the SM g-factor analysis, we examine the NPA wave functions and compare them with the seniority-2 configurations $(0h_{11/2})^{-2}_\nu$ and $(0h_{11/2})^2_\pi$, and the seniority-4 configuration $6^+_\pi \otimes 2^+_\nu$. In the NPA, the higher-seniority configurations are effectively constructed

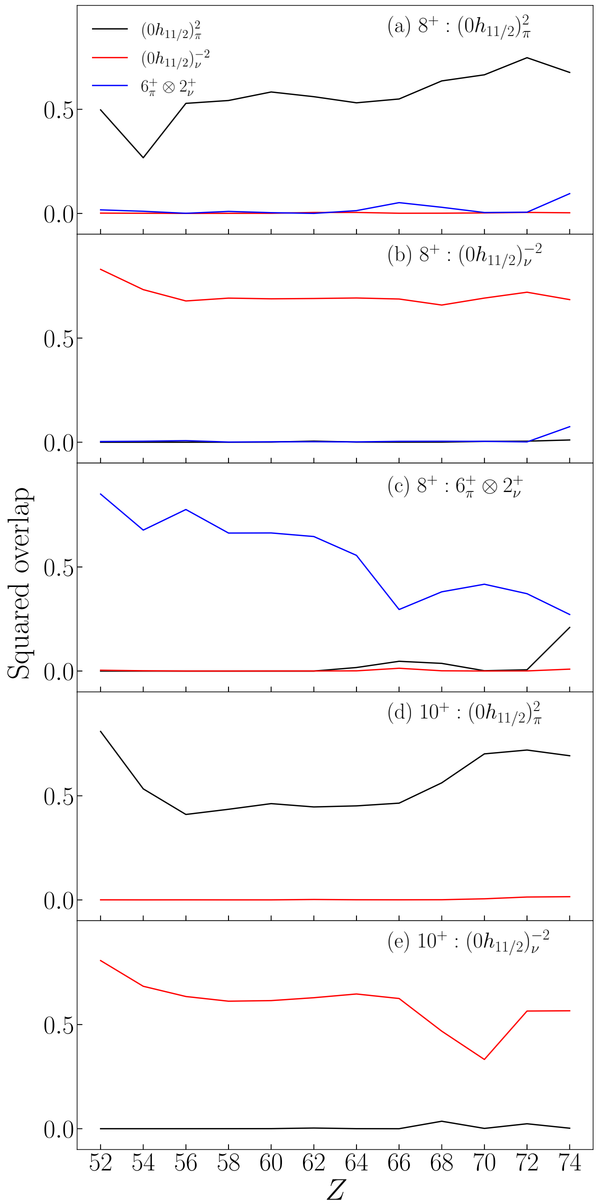

FIG. 7: Squared overlaps between the full NPA wave functions and the wave function of a single configuration $[(0h_{11/2})^{-2}_\nu$, $6^+_\pi \otimes 2^+_\nu$, or $(0h_{11/2})^2_\pi]$ normalized to unit norm, for the low-lying 8^+ and 10^+ states along the $N = 80$ isotones. The solid black, red, and blue curves represent the proton $(0h_{11/2})^2_\pi$, neutron $(0h_{11/2})^{-2}_\nu$, and proton-neutron coupled $6^+_\pi \otimes 2^+_\nu$ configurations, respectively. Panels (a)-(c) show the three 8^+ states, and panels (d) and (e) show the two 10^+ states.

from the S-pair condensate with one or more broken pairs. Fig. 7 shows the probabilities of these configurations in the NPA wave functions for the 8^+ and 10^+ states. The 8^+ and 10^+ states examined in Fig. 7 are the same states whose g-factors and excitation energies are shown in Figs. 5 and 6. Our discussion below focuses on the configuration that dominates each state. For the 8^+ states, the dominant configurations typically contribute about 50%-85% of the total wave function. In ^{148}Er-^{154}W, however, the $6^+_\pi \otimes 2^+_\nu$ configuration contributes 30%-40%, indicating more pronounced mixing. For the 10^+ states, the proton $(0h_{11/2})^2_\pi$ configuration contributes 40%-80%, while the neutron $(0h_{11/2})^{-2}_\nu$ component remains 30%-80%. Overall, the yrast 8^+ and 10^+ states exhibit a larger contribution from a single configuration, while non-yrast states show smaller percentages. This reflects stronger configuration mixing at higher excitation energies.

It may be interesting to note that, though not shown, the NPA calculation also indicates small contributions from seniority-4 components other than $6^+_\pi \otimes 2^+_\nu$: the 8^+ states dominated by $(0h_{11/2})^{-2}_\nu$ contain about 5%-10% of the $2^+_\pi \otimes 6^+_\nu$ configuration, the 10^+ states dominated by $(0h_{11/2})^{-2}_\nu$ contain about 10%-25% of the $2^+_\pi \otimes 10^+_\nu$ configuration, and the 10^+ states dominated by $(0h_{11/2})^2_\pi$ contain 1%-22% of the $10^+_\pi \otimes 2^+_\nu$ configuration.

As noted in Sec. III A, the SM $B(E2)$ values, shown in Fig. 1(a) and Table I, are overall consistent with experiment. However, their magnitudes cannot be fully explained by the dominant configurations or the seniority-4 components in our NPA calculation. This indicates that the $B(E2)$ strengths are strongly influenced by configuration mixing from minor components (e.g., seniority-6 or higher).

E. A level inversion in ^{154}W

Finally, we discuss an intriguing phenomenon predicted by our SM calculation in ^{154}W. Fig. 8 shows the systematics of the excitation energies for the yrast 18^+ and 20^+ states in ^{132}Te-^{154}W, and the SM result agrees well with available experimental data. In all isotones, the 20^+ level lies above the 18^+ level, except in ^{154}W, where the 20^+ state is predicted to lie 0.2 MeV below the 18^+ level, suggesting the occurrence of a level inversion.

The SM calculation indicates that the yrast 18^+ and 20^+ states in ^{154}W are essentially two-proton-hole states in the $0h_{11/2}$ orbital, since the $0g_{7/2}$ and $1d_{5/2}$ orbitals are nearly filled, and the $1d_{3/2}$ and $2s_{1/2}$ orbitals are almost empty, leaving ten valence protons to occupy the $0h_{11/2}$ orbital. The two valence neutron holes occupy mostly the $0h_{11/2}$ orbital as well. As a result, these states can be approximated as the maximally aligned coupling of two proton holes and two neutron holes within the same $0h_{11/2}$ orbital. We performed a SM calculation with the isoscalar spin-aligned $J = 11$ proton-neutron matrix element switched off. In this case, the 20^+ level lies 0.4

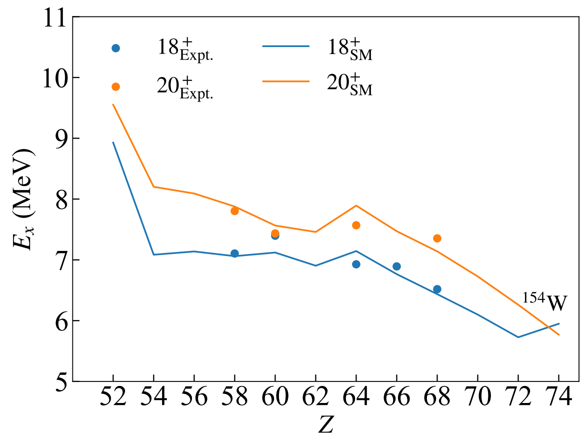

FIG. 8: Systematics of the yrast 18^+ and 20^+ states in the $N = 80$ isotones. The SM calculation predicts a level inversion between these two states in ^{154}W.

MeV above the 18^+ level, confirming that the isoscalar spin-aligned interaction is essential for the emergence of the level inversion in ^{154}W.

A similar mechanism is known for the "level-inversion" 16^+ isomer in ^{96}Cd [94]. ^{96}Cd can be viewed as two proton holes and two neutron holes in the $0g_{9/2}$ orbital below the ^{100}Sn core. Ref. [94] reports that the isoscalar proton-neutron interaction plays a crucial role in reproducing this inversion. Theoretical studies reveal that the yrast 14^+ and 16^+ states in ^{96}Cd can be described predominantly by isoscalar spin-aligned $J = 9$ proton-neutron pairs [95–100].

This analogy highlights the microscopic origin of the predicted level inversion in ^{154}W and indicates that the proximity of both proton and neutron Fermi surfaces to high-j orbitals, combined with strong isoscalar spin-aligned interactions, may favor similar level inversions in other nuclei with two proton holes and two neutron holes occupying such orbitals. Although a detailed study of the electromagnetic transitions of the 20^+ state to odd-parity states are beyond the scope of the present work, the predicted level inversion suggests that this state could exhibit suppressed decays to even-parity states, potentially forming a long-lived 20^+ isomer. Such a state could allow measurable beta decays and provide guidance for future experimental studies.

IV. SUMMARY

In this work, we have investigated the systematics of low-lying even-parity states in the $N = 80$ even-even isotones ^{130}Sn-^{154}W using large-scale SM calculations with an optimized effective interaction. The proton-proton and neutron-neutron interactions are adopted from previous works that successfully describe semi-magic nuclei, whereas the proton-neutron interaction is newly optimized by fitting 14 correction terms to 73 experimental excitation energies in the $N = 80$ and 81 isotones. The parameter space is reduced to eight independent degrees of freedom using the PCA method. The calculations well reproduce the excitation energies and electromagnetic properties of the low-lying states in the $N = 80$ isotones, as well as the lowest-energy $3/2^+$, $1/2^+$, and $11/2^-$ states in the $N = 81$ isotones.

SM results indicate that the coexistence of collective, weak-coupling, and seniority-type states is a robust feature of the low-lying structures along the $N = 80$ isotonic chain. Specifically, the yrast 0^+, 2^+, and 4^+ states in ^{130}Sn are dominated by seniority-type configurations, while those in ^{134}Xe-^{154}W show vibrational-like features. The yrast 6^+ state in ^{130}Sn is dominated by neutron $(0h_{11/2})^{-2}_{\nu}$ configuration, whereas for $Z > 50$ it is dominated by proton seniority-2 configurations, $6^+_{\pi} \otimes 0^+_{\nu}$. Three types of low-lying 8^+ states are identified in calculations: neutron $(0h_{11/2})^{-2}_{\nu}$, proton-neutron coupled $6^+_{\pi} \otimes 2^+_{\nu}$, and proton seniority-2 $(0h_{11/2})^2_{\pi}$. Their evolutions reflects the interplay between the proton Fermi surface and neutron shell evolution driven by the proton-neutron monopole interaction. Similarly, $(0h_{11/2})^{-2}_{\nu}$ and $(0h_{11/2})^2_{\pi}$ 10^+ states are predicted, showing a configuration transition along the yrast states. The NPA analysis quantitatively confirms the SM interpretation. A level inversion of the yrast 18^+ and 20^+ states is predicted in ^{154}W, revealing the essential role of the isoscalar spin-aligned $J = 11$ proton-neutron coupling and indicating that this 20^+ state may be a long-lived isomer, similar to the 16^+ spin-trap isomer in ^{96}Cd.

These results provide a comprehensive picture of structure evolution along the $N = 80$ isotonic chain and suggest intriguing features for future experimental investigations. The present study also provides a solid foundation for extending analysis to more neutron-deficient nuclei near $N \approx 80$, as well as to nuclei with smaller N approaching Z, where exotic phenomena such as rapid shape-phase transitions and enhanced isoscalar proton-neutron pairing correlations may appear. Moreover, the PCA-based monopole- and multipole-optimization approach for effective interactions can be extended to heavier open-shell nuclei in the vicinity of ^{208}Pb, offering a powerful tool for future theoretical studies.

Acknowledgments

We are grateful to Prof. Y. M. Zhao and Prof. P. M. Walker for their careful reading of the paper and valuable comments. This work is supported by the National Natural Science Foundation of China under Grant Nos. 12322506, 12535009, 12075169, 12505140, 12405140, and 12135004. C.Q. acknowledges the support from the Olle Engkvist Foundation. C.W.J. acknowledges the support from the U.S. Department of Energy, Office of Science, Office of Nuclear Physics, under Award No. DE-FG02-03ER41272, and from the CUSTIPEN (China-U.S. Theory Institute for Physics with Exotic Nuclei) funded by the U.S. Department of Energy, Office of Science, under Grant No. DE-SC0009971. A.A. acknowledges the support from the UK STFC, and from the Chinese Academy of Sciences President's International Fellowship Initiative under Grant Nos. 2025PVB0082 and 2020VMA0017. This work is also supported by the Hebei Natural Science Foundation of China under Grant No. A2025203002; the Natural Science Foundation of Gansu Province of China under Grant No. 24JRRA033; and the Fundamental Research Funds for the Central Universities. We also acknowledge the support of Tongji University Intelligent Computing Center.

Appendix A: Tables of $B(E2)$ values and g-factors

Given the overall agreement between the experimental data and the SM calculations, we present comprehensive tables of $B(E2)$ transition strengths and magnetic g-factors for low-lying states in the $N = 80$ even-even isotones.

TABLE I: Experimental and calculated $B(E2)$ values (in W.u.). Listed are the $E2$ transitions between the yrast states, together with additional transitions for which experimental data are available. For ^{142}Sm and ^{144}Gd, the transitions from the 10_2^+ states to several lower-lying final states are also included because the predicted partial half-lives of the 10_2^+ states exceed 10^{-7} s. The SM $B(E2)$ values are calculated using effective charges $e_\pi = 1.5e$ and $e_\nu = 1.1e$. The table also lists the experimental half-lives $T_{1/2,\mathrm{Expt.}}$ (in s) for the parent states and the partial half-lives for the $E2$ transitions obtained from the SM, $T_{1/2,\mathrm{SM}}^{(E2)}$. The $T_{1/2,\mathrm{SM}}^{(E2)}$ values are calculated using the experimental γ-ray energies when available; values in parentheses correspond to transitions for which the γ-ray energy is not measured and thus the SM-calculated energy is used.

Nuclide	$I^\pi \to J^\pi$	$B(E2)_{\mathrm{Expt.}}$	$T_{1/2,\mathrm{Expt.}}$ (in s)	$B(E2)_{\mathrm{SM}}$	$T_{1/2,\mathrm{SM}}^{(E2)}$ (in s)
^{130}Sn	$2_1^+ \to 0_1^+$			3.423	1.557×10^{-12}
	$4_1^+ \to 2_1^+$			2.823	1.844×10^{-11}
	$6_1^+ \to 4_1^+$			2.751	4.340×10^{-9}
	$8_1^+ \to 6_1^+$		$< 4 \times 10^{-8}$	1.743	2.238×10^{-6}
	$10_1^+ \to 8_1^+$	0.38(4)	$1.61(15) \times 10^{-6}$	0.656	2.705×10^{-6}
^{132}Te	$2_1^+ \to 0_1^+$	10.82(110)	$1.83(18) \times 10^{-12}$	9.232	2.015×10^{-12}
	$4_1^+ \to 2_1^+$			7.322	9.729×10^{-12}
	$6_1^+ \to 4_1^+$	3.3(2)	$1.45(8) \times 10^{-7}$	2.963	4.125×10^{-7}
	$8_1^+ \to 6_1^+$			0.0274	7.561×10^{-10}
	$10_1^+ \to 8_1^+$		$3.70(9) \times 10^{-6}$	1.372	2.004×10^{-3}
	$2_2^+ \to 0_1^+$	0.5(1)		0.310	3.575×10^{-12}
^{134}Xe	$2_1^+ \to 0_1^+$	15.32(103)	$2.08(14) \times 10^{-12}$	12.229	2.605×10^{-12}
	$4_1^+ \to 2_1^+$	11.6(8)	$2.22(14) \times 10^{-12}$	14.380	1.789×10^{-12}
	$6_1^+ \to 4_1^+$			5.948	2.116×10^{-10}
	$8_1^+ \to 6_1^+$			11.879	2.485×10^{-12}
	$10_1^+ \to 8_1^+$		$5(1) \times 10^{-6}$	0.0232	3.485×10^{-2}
	$2_2^+ \to 2_1^+$	20(2)		5.044	1.044×10^{-11}
	$2_2^+ \to 0_1^+$	0.75(5)		3.047	4.174×10^{-13}
^{136}Ba	$2_1^+ \to 0_1^+$	19.59(34)	$1.89(3) \times 10^{-12}$	14.597	2.532×10^{-12}
	$4_1^+ \to 2_1^+$	14(6)	$0.87(^{+84}_{-29}) \times 10^{-12}$	19.033	5.659×10^{-13}
	$6_1^+ \to 4_1^+$	0.55(2)	$3.1(1) \times 10^{-9}$	0.657	4.559×10^{-9}
	$8_1^+ \to 6_1^+$			6.745	6.686×10^{-12}
	$10_1^+ \to 8_1^+$	0.0232(6)	$9.1(2) \times 10^{-8}$	0.00474	4.542×10^{-7}
	$2_2^+ \to 2_1^+$	17(6)	$8.9(29) \times 10^{-13}$	8.940	7.297×10^{-12}

	$2_2^+ \to 0_1^+$	0.89(25)		5.277	2.884×10^{-13}
	$4_1^+ \to 2_2^+$	1.4(6)		0.451	9.423×10^{-9}
	$4_2^+ \to 2_1^+$	5(3)		3.881	1.226×10^{-12}
	$6_1^+ \to 4_2^+$	4.9(4)		1.658	9.484×10^{-8}
^{138}Ce	$2_1^+ \to 0_1^+$	21.6(16)	$1.98(4) \times 10^{-12}$	18.369	2.378×10^{-12}
	$4_1^+ \to 2_1^+$		$< 4 \times 10^{-11}$	25.855	4.307×10^{-13}
	$6_1^+ \to 4_1^+$	$0.105(^{+18}_{-16})$	$8.80(19) \times 10^{-10}$	2.105	2.826×10^{-10}
	$8_1^+ \to 6_1^+$			21.618	1.718×10^{-12}
	$10_1^+ \to 8_1^+$	0.0108(3)	$8.2(2) \times 10^{-8}$	0.0128	7.076×10^{-8}
	$2_2^+ \to 0_1^+$	1.15(4)	$8.34(20) \times 10^{-13}$	5.655	3.008×10^{-13}
	$6_1^+ \to 4_2^+$	$6.1(^{+9}_{-8})$		0.435	3.215×10^{-7}
^{140}Nd	$2_1^+ \to 0_1^+$	33.6(2)	$1.40(11) \times 10^{-12}$	21.641	2.179×10^{-12}
	$4_1^+ \to 2_1^+$			30.640	3.724×10^{-13}
	$6_1^+ \to 4_1^+$			0.308	7.458×10^{-10}
	$8_1^+ \to 6_1^+$			20.892	1.702×10^{-12}
	$10_1^+ \to 8_1^+$	0.0013(2)	$2.7(5) \times 10^{-8}$	0.000457	1.786×10^{-6}
^{142}Sm	$2_1^+ \to 0_1^+$			22.642	2.125×10^{-12}
	$4_1^+ \to 2_1^+$			33.219	3.454×10^{-13}
	$6_1^+ \to 4_1^+$		$< 2 \times 10^{-9}$	0.0399	3.269×10^{-9}
	$8_1^+ \to 6_1^+$			18.135	1.161×10^{-12}
	$10_1^+ \to 8_1^+$		$4.80(60) \times 10^{-7}$	0.000156	2.281×10^{-5}
	$10_1^+ \to 8_2^+$			0.326	(4.933×10^{-5})
	$10_2^+ \to 8_1^+$			0.00353	1.158×10^{-7}
	$10_2^+ \to 8_2^+$			0.00497	(3.310×10^{-5})
	$10_2^+ \to 10_1^+$			0.207	5.240×10^{-7}
^{144}Gd	$2_1^+ \to 0_1^+$			23.866	2.335×10^{-12}
	$4_1^+ \to 2_1^+$			37.053	3.388×10^{-13}
	$6_1^+ \to 4_1^+$			0.0999	1.495×10^{-9}
	$8_1^+ \to 6_1^+$			4.330	(2.451×10^{-11})
	$8_1^+ \to 10_1^+$			2.639	(3.077×10^{-3})
	$10_1^+ \to 8_1^+$		$1.45(30) \times 10^{-7}$	2.136	
	$10_2^+ \to 8_1^+$			0.0105	(1.223×10^{-7})
	$10_2^+ \to 8_2^+$			0.0000544	(8.9128×10^{-5})
	$10_2^+ \to 10_1^+$			0.0451	2.184×10^{-7}
^{146}Dy	$2_1^+ \to 0_1^+$			27.624	3.039×10^{-12}
	$4_1^+ \to 2_1^+$			44.166	4.142×10^{-13}
	$6_1^+ \to 4_1^+$			0.635	4.372×10^{-11}
	$8_1^+ \to 6_1^+$			10.476	2.882×10^{-11}
	$8_1^+ \to 10_1^+$			1.376	2.368×10^{-5}
	$10_1^+ \to 8_1^+$		0.150(20)	1.113	
^{148}Er	$2_1^+ \to 0_1^+$			30.429	3.581×10^{-12}
	$4_1^+ \to 2_1^+$			48.171	4.868×10^{-13}
	$6_1^+ \to 4_1^+$			20.581	5.823×10^{-13}
	$8_1^+ \to 6_1^+$			8.083	1.342×10^{-9}
	$10_1^+ \to 8_1^+$	0.012(3)	$1.3(3) \times 10^{-5}$	0.146	2.158×10^{-6}
^{150}Yb	$2_1^+ \to 0_1^+$			30.486	3.737×10^{-12}
	$4_1^+ \to 2_1^+$			46.518	5.557×10^{-13}
	$6_1^+ \to 4_1^+$			40.467	3.351×10^{-13}
	$8_1^+ \to 6_1^+$			27.155	2.073×10^{-10}
	$10_1^+ \to 8_1^+$	0.36(3)	$6.2(5) \times 10^{-7}$	4.343	1.633×10^{-8}
^{152}Hf	$2_1^+ \to 0_1^+$			26.880	(2.696×10^{-12})
	$4_1^+ \to 2_1^+$			38.460	(4.641×10^{-13})
	$6_1^+ \to 4_1^+$			31.584	(2.406×10^{-12})
	$8_1^+ \to 6_1^+$			18.745	(3.844×10^{-10})
	$10_1^+ \to 8_1^+$			27.591	(7.312×10^{-7})

^{154}W	$2_1^+ \to 0_1^+$			20.415	(2.174×10^{-12})
	$4_1^+ \to 2_1^+$			23.504	(4.997×10^{-13})
	$6_1^+ \to 4_1^+$			21.589	(1.953×10^{-11})
	$8_1^+ \to 6_1^+$			19.962	(5.502×10^{-9})
	$10_1^+ \to 8_1^+$			15.475	(6.152×10^{-8})

TABLE II: Experimental and calculated g-factors for low-lying states in the $N = 80$ isotones. For each nucleus we list the yrast 2^+, 4^+, and 6^+ states, the 8^+ states dominated by the $(0h_{11/2})_\nu^{-2}$, $6_\pi^+ \otimes 2_\nu^+$, and $(0h_{11/2})_\pi^2$ configurations, and the 10^+ states dominated by the $(0h_{11/2})_\nu^{-2}$ and $(0h_{11/2})_\pi^2$ configurations.

Nuclide	I^π	$g_{\rm Expt.}$	$g_{\rm SM}$
^{130}Sn	2_1^+	-	-0.167
	4_1^+	-	-0.230
	6_1^+	-	-0.243
	8_1^+	-	-0.243
	10_1^+	-	-0.243
^{132}Te	2_1^+	-	0.171
	4_1^+	-	0.592
	6_1^+	0.783(83)	0.664
	8_1^+	-	-0.210
	8_2^+	-	0.449
	10_1^+	-	-0.222
^{134}Xe	2_1^+	0.354(7)	0.158
	4_1^+	0.80(15)	0.413
	6_1^+	-	0.666
	8_1^+	-	0.519
	8_2^+	-	-0.158
	10_1^+	-	-0.204
^{136}Ba	2_1^+	0.34(5)	0.152
	4_1^+	-	0.383
	6_1^+	-	0.967
	8_1^+	-	0.559
	8_3^+	-	-0.150
	8_{43}^+	-	0.957
	10_1^+	-	-0.191
	10_{13}^+	-	1.098
^{138}Ce	2_1^+	0.26(8)	0.216
	4_1^+	-	0.446
	6_1^+	-	0.975
	8_1^+	-	0.801
	8_3^+	-	-0.133
	8_{17}^+	-	1.131
	10_1^+	-0.170(3)	-0.179
	10_5^+	-	1.208
^{140}Nd	2_1^+	-	0.260
	4_1^+	-	0.432
	6_1^+	-	0.968
	8_1^+	-	0.785
	8_3^+	-	-0.113
	8_8^+	-	1.137
	10_1^+	-0.192(12)	-0.164
	10_3^+	-	1.220
^{142}Sm	2_1^+	-	0.255
	4_1^+	-	0.366
	6_1^+	-	0.950
	8_1^+	-	0.753
	8_3^+	-	-0.047
	8_4^+	-	1.178
	10_1^+	-	-0.144
	10_2^+	-	1.217
^{144}Gd	2_1^+	-	0.266
	4_1^+	-	0.341
	6_1^+	-	0.960
	8_1^+	-	1.155
	8_2^+	-	0.844
	8_4^+	-	-0.034
	10_1^+	1.276(14)	1.213
	10_2^+	-	-0.122
^{146}Dy	2_1^+	-	0.347
	4_1^+	-	0.433
	6_1^+	-	1.138
	8_1^+	-	1.187
	8_3^+	-	1.002
	8_5^+	-	0.065
	10_1^+	-	1.206
	10_3^+	-	-0.078
^{148}Er	2_1^+	-	0.436
	4_1^+	-	0.589
	6_1^+	-	1.093
	8_1^+	-	1.186
	8_3^+	-	1.035
	8_6^+	-	0.322
	10_1^+	-	1.202
	10_4^+	-	0.098
^{150}Yb	2_1^+	-	0.499
	4_1^+	-	0.723
	6_1^+	-	1.040
	8_1^+	-	1.168
	8_4^+	-	1.052
	8_7^+	-	0.167
	10_1^+	-	1.187
	10_4^+	-	0.016
^{152}Hf	2_1^+	-	0.483
	4_1^+	-	0.785
	6_1^+	-	1.074
	8_1^+	-	1.190
	8_4^+	-	1.053
	8_6^+	-	0.127
	10_1^+	-	1.171
	10_4^+	-	0.025
^{154}W	2_1^+	-	0.376
	4_1^+	-	0.878
	6_1^+	-	1.137

8_1^+	-	1.182
8_3^+	-	0.992
8_4^+	-	0.149
10_1^+	-	1.156
10_4^+	-	0.099

[1] K. Ortner, C. Andreoiu, C. M. Petrache, C. Qi, A. Astier, T. D. Bucher, G. Colombi, E. Dupont, F. H. Garcia, P. E. Garrett, S. Guo, G. Häfner, B. Jigmeddorj, J. Jolie, F. Kandzia, V. Karayonchev, Y.-H. Kim, L. Knafla, B. F. Lv, N. Mărginean, E. McGee, C. Michelagnoli, C. Mihai, P. Mutti, C. Porzio, K. Raymond, J.-M. Régis, N. Saed-Samii, P. Spagnoletti, W. Urban, S. Valbuena, J. R. Vanhoy, K. Whitmore, J. Wisniewski, and S. W. Yates, Phys. Rev. C **109**, 054317 (2024).

[2] E. A. Cederlöf, T. Bäck, J. Nyberg, C. Qi, A. Ataç, H. Badran, T. Braunroth, T. Calverley, D. Cox, M. Doncel, *et al.*, The European Physical Journal A **59**, 300 (2023).

[3] M. Storbacka and C. Qi, Physics Letters B **855**, 138822 (2024).

[4] M. Doncel, T. Bäck, C. Qi, D. M. Cullen, D. Hodge, B. Cederwall, M. J. Taylor, M. Procter, M. Giles, K. Auranen, T. Grahn, P. T. Greenlees, U. Jakobsson, R. Julin, S. Juutinen, A. Herzáň, J. Konki, J. Pakarinen, J. Partanen, P. Peura, P. Rahkila, P. Ruotsalainen, M. Sandzelius, J. Sarén, C. Scholey, J. Sorri, S. Stolze, and J. Uusitalo, Phys. Rev. C **96**, 051304 (2017).

[5] Y. Y. Cheng, C. Qi, Y. M. Zhao, and A. Arima, Phys. Rev. C **94**, 024321 (2016).

[6] M. Doncel, T. Bäck, D. M. Cullen, D. Hodge, C. Qi, B. Cederwall, M. J. Taylor, M. Procter, K. Auranen, T. Grahn, P. T. Greenlees, U. Jakobsson, R. Julin, S. Juutinen, A. Herzán, J. Konki, M. Leino, J. Pakarinen, J. Partanen, P. Peura, P. Rahkila, P. Ruotsalainen, M. Sandzelius, J. Sarén, C. Scholey, J. Sorri, S. Stolze, and J. Uusitalo, Phys. Rev. C **91**, 061304 (2015).

[7] H. Jiang, C. Qi, Y. Lei, R. Liotta, R. Wyss, and Y. M. Zhao, Phys. Rev. C **88**, 044332 (2013).

[8] T. Bäck, C. Qi, B. Cederwall, R. Liotta, F. Ghazi Moradi, A. Johnson, R. Wyss, and R. Wadsworth, Phys. Rev. C **87**, 031306 (2013).

[9] M. G. Procter, D. M. Cullen, M. J. Taylor, J. Pakarinen, K. Auranen, T. Bäck, T. Braunroth, B. Cederwall, A. Dewald, T. Grahn, P. T. Greenlees, U. Jakobsson, R. Julin, S. Juutinen, A. Herzáň, J. Konki, M. Leino, R. Liotta, J. Partanen, P. Peura, P. Rahkila, P. Ruotsalainen, M. Sandelius, J. Sarén, C. Scholey, J. Sorri, S. Stolze, J. Uusitalo, and C. Qi, Phys. Rev. C **87**, 014308 (2013).

[10] C. Qi and Z. X. Xu, Phys. Rev. C **86**, 044323 (2012).

[11] C. Qi, Phys. Rev. C **94**, 034310 (2016).

[12] C. Qi, Journal of Physics: Conference Series **742**, 012030 (2016).

[13] T. Faestermann, H. Bohn, F. Feilitzsch, A. Sunyar, R. Broda, P. Kleinheinz, and M. Ogawa, Physics Letters B **80**, 190 (1979).

[14] B. Bhoy and P. C. Srivastava, Journal of Physics G: Nuclear and Particle Physics **49**, 085101 (202

[15] S. Beck, B. Kootte, I. Dedes, T. Dickel, A. A. Kwiatkowski, E. M. Lykiardopoulou, W. R. Plaß, M. P. Reiter, C. Andreoiu, J. Bergmann, T. Brunner, D. Curien, J. Dilling, J. Dudek, E. Dunling, J. Flowerdew, A. Gaamouci, L. Graham, G. Gwinner, A. Jacobs, R. Klawitter, Y. Lan, E. Leistenschneider, N. Minkov, V. Monier, I. Mukul, S. F. Paul, C. Scheidenberger, R. I. Thompson, J. L. Tracy, M. Vansteenkiste, H.-L. Wang, M. E. Wieser, C. Will, and J. Yang, Phys. Rev. Lett. **127**, 112501 (2021).

[16] W. Q. Zhang, Z. Liu, A. N. Andreyev, Y. X. Yu, G. J. Fu, C. Qi, H. Huang, X. H. Yu, P. M. Walker, X. H. Zhou, P. T. Greenlees, R. D. Page, B. H. Sun, S. F. Ashley, I. G. Darby, S. Eeckhaudt, A. B. Garnsworthy, M. B. Gómez-Hornillos, T. Grahn, D. G. Jenkins, P. Jones, R. Julin, D. T. Joss, S. Ketelhut, J. G. Li, M. Leino, M. L. Liu, Z. H. Li, C. Ma, M. Niikura, M. Nyman, J. Pakarinen, S. Pietri, Z. Podolyák, P. Rahkila, J. Sarén, N. J. Thompson, J. Uusitalo, T. Uesaka, S. Williams, Y. F. Wu, X. X. Xu, C. X. Yuan, Q. B. Zeng, F. S. Zhang, and S. Y. Zhang, Phys. Rev. Lett. **136**, 082503 (2026).

[17] H. B. Yang, Z. G. Gan, Y. J. Li, M. L. Liu, S. Y. Xu, C. Liu, M. M. Zhang, Z. Y. Zhang, M. H. Huang, C. X. Yuan, S. Y. Wang, L. Ma, J. G. Wang, X. C. Han, A. Rohilla, S. Q. Zuo, X. Xiao, X. B. Zhang, L. Zhu, Z. F. Yue, Y. L. Tian, Y. S. Wang, C. L. Yang, Z. Zhao, X. Y. Huang, Z. C. Li, L. C. Sun, J. Y. Wang, H. R. Yang, Z. W. Lu, W. Q. Yang, X. H. Zhou, W. X. Huang, N. Wang, S. G. Zhou, Z. Z. Ren, and H. S. Xu, Phys. Rev. Lett. **132**, 072502 (2024).

[18] A. Briscoe, R. Page, J. Uusitalo, D. Joss, M. AlAqeel, B. Alayed, B. Andel, S. Antalic, K. Auranen, H. Ayatollahzadeh, H. Badran, L. Barber, G. Beeton, M. Birova, V. Bogdanoff, R. Clark, J. Cubiss, D. Cullen, J. Deary, U. Forsberg, T. Grahn, P. Greenlees, J. Hilton, A. Illana, H. Joukainen, D. Judson, R. Julin, H. Jutila, J. Keatings, M. Labiche, M. Leino, M. Lewis, J. Louko, M. Luoma, I. Martel, A. McCarter, P. McKee, P. Mosat, S. Nathaniel, O. Neuvonen, D. O'Donnell, J. Ojala, C. Page, A. Plaza, J. Pakarinen, P. Papadakis, E. Parr, J. Partanen, P. Rahkila, P. Ruotsalainen, M. Sandzelius, J. Sarén, B. Saygi, J. Smallcombe, J. Smith, J. Sorri, C. Sullivan, S. Szwec, H. Tann, A. Tolosa-Delgado, E. Uusikylä, M. Venhart, L. Waring, and G. Zimba, Physics Letters B **847**, 138310 (2023).

[19] I. Talmi, *Simple models of complex nuclei: the shell*

model and the interacting boson model (CRC Press, 1993).

[20] I. Talmi, International Journal of Modern Physics E **14**, 821 (2005).

[21] B. Brown, Progress in Particle and Nuclear Physics **47**, 517 (2001).

[22] E. Caurier, G. Martínez-Pinedo, F. Nowacki, A. Poves, and A. P. Zuker, Rev. Mod. Phys. **77**, 427 (2005).

[23] M. Liu and C. Yuan, International Journal of Modern Physics E **32**, 2330003 (2023).

[24] A. Holt, T. Engeland, E. Osnes, M. Hjorth-Jensen, and J. Suhonen, Nuclear Physics A **618**, 107 (1997).

[25] J. Suhonen, J. Toivanen, A. Holt, T. Engeland, E. Osnes, and M. Hjorth-Jensen, Nuclear Physics A **628**, 41 (1998).

[26] L. Coraggio, A. Covello, A. Gargano, N. Itaco, and T. T. S. Kuo, Phys. Rev. C **80**, 044320 (2009).

[27] Q. Y. Chen, Y. X. Yu, S. T. Guo, G. J. Fu, and Z. Z. Ren, Nuclear Physics Review **41**, 606 (2024).

[28] Y. X. Yu, Q. Y. Chen, C. Qi, and G. J. Fu, Phys. Rev. C **113**, 024318 (2026).

[29] A. Vogt, B. Birkenbach, P. Reiter, A. Blazhev, M. Siciliano, K. Hadyńska-Klęk, J. J. Valiente-Dobón, C. Wheldon, E. Teruya, N. Yoshinaga, K. Arnswald, D. Bazzacco, M. Bowry, A. Bracco, B. Bruyneel, R. S. Chakrawarthy, R. Chapman, D. Cline, L. Corradi, F. C. L. Crespi, M. Cromaz, G. de Angelis, J. Eberth, P. Fallon, E. Farnea, E. Fioretto, S. J. Freeman, B. Fu, A. Gadea, K. Geibel, W. Gelletly, A. Gengelbach, A. Giaz, A. Görgen, A. Gottardo, A. B. Hayes, H. Hess, R. Hirsch, H. Hua, P. R. John, J. Jolie, A. Jungclaus, L. Kaya, W. Korten, I. Y. Lee, S. Leoni, L. Lewandowski, X. Liang, S. Lunardi, A. O. Macchiavelli, R. Menegazzo, D. Mengoni, C. Michelagnoli, T. Mijatović, G. Montagnoli, D. Montanari, C. Müller-Gatermann, D. Napoli, C. J. Pearson, L. Pellegri, Z. Podolyák, G. Pollarolo, A. Pullia, M. Queiser, F. Radeck, F. Recchia, P. H. Regan, D. Rosiak, N. Saed-Samii, E. Şahin, F. Scarlassara, D. Schneiders, M. Seidlitz, B. Siebeck, G. Sletten, J. F. Smith, P.-A. Söderström, A. M. Stefanini, T. Steinbach, O. Stezowski, S. Szilner, B. Szpak, R. Teng, C. Ur, V. Vandone, D. D. Warner, A. Wiens, C. Y. Wu, and K. O. Zell, Phys. Rev. C **95**, 024316 (2017).

[30] K. Heyde and P. J. Brussaard, Zeitschrift für Physik A Hadrons and nuclei **259**, 15 (1973).

[31] K. S. Toth, Y. A. Ellis-Akovali, F. T. Avignone, R. S. Moore, D. M. Moltz, J. M. Nitschke, P. A. Wilmarth, P. K. Lemmertz, D. C. Sousa, and A. L. Goodman, Phys. Rev. C **32**, 342 (1985).

[32] K. Sieja, G. Martínez-Pinedo, L. Coquard, and N. Pietralla, Phys. Rev. C **80**, 054311 (2009).

[33] D. Bianco, F. Andreozzi, N. Lo Iudice, A. Porrino, and F. Knapp, Phys. Rev. C **85**, 034332 (2012).

[34] M. Bao, H. Jiang, Y. M. Zhao, and A. Arima, Phys. Rev. C **101**, 014316 (2020).

[35] C. Ma, Y. X. Yu, X. Yin, G. J. Fu, and Y. M. Zhao, Phys. Rev. C **112**, 014323 (2025).

[36] K. Pearson, The London, Edinburgh, and Dublin Philosophical Magazine and Journal of Science **2**, 559 (1901).

[37] H. Hotelling, Journal of Educational Psychology **24**, 417– (1933).

[38] I. T. Jolliffe and J. Cadima, Philosophical Transactions of the Royal Society A **374**, 20150202 (2

[39] C. W. Johnson, W. E. Ormand, and P. G. Krastev, Computer Physics Communications **184**, 2761 (2013).

[40] C. W. Johnson, W. E. Ormand, K. S. McElvain, and H. Shan, Bigstick: A flexible configuration-interaction shell-model code (2018), arXiv:1801.08432 [physics.comp-ph] .

[41] Q. Y. Chen, *Study of low-lying states of nuclei in the medium-heavy region based on the effective interaction (in Chinese)*, Master's thesis, Tongji University, Shanghai (2023).

[42] B. Brown and W. Rae, Nuclear Data Sheets **120**, 115 (2014).

[43] S. P. Pandya, Phys. Rev. **103**, 956 (1956).

[44] A. Arima, S. Cohen, R. Lawson, and M. MacFarlane, Nuclear Physics A **108**, 94 (1968).

[45] W. Richter, M. Van Der Merwe, R. Julies, and B. Brown, Nuclear Physics A **523**, 325 (1991).

[46] M. Honma, B. Brown, T. Mizusaki, and T. Otsuka, Nuclear Physics A **704**, 134 (2002), rIKEN Symposium Shell Model 2000.

[47] M. Honma, T. Otsuka, B. A. Brown, and T. Mizusaki, Phys. Rev. C **65**, 061301 (2002).

[48] A. F. Lisetskiy, B. A. Brown, M. Horoi, and H. Grawe, Phys. Rev. C **70**, 044314 (2004).

[49] B. A. Brown and W. A. Richter, Phys. Rev. C **74**, 034315 (2006).

[50] M. Honma, T. Otsuka, T. Mizusaki, and M. Hjorth-Jensen, Phys. Rev. C **80**, 064323 (2009).

[51] Y. Khazov, A. Rodionov, S. Sakharov, and B. Singh, Nuclear Data Sheets **104**, 497 (2005).

[52] A. Sonzogni, Nuclear Data Sheets **103**, 1 (2004).

[53] E. Mccutchan, Nuclear Data Sheets **152**, 331 (2018).

[54] J. Chen, Nuclear Data Sheets **146**, 1 (2017).

[55] N. Nica, Nuclear Data Sheets **154**, 1 (2018).

[56] T. Johnson, D. Symochko, M. Fadil, and J. Tuli, Nuclear Data Sheets **112**, 1949 (2011).

[57] N. Nica, Nuclear Data Sheets **117**, 1 (2014).

[58] Y. Khazov, A. Rodionov, and F. Kondev, Nuclear Data Sheets **112**, 855 (2011).

[59] B. Singh, A. A. Rodionov, and Y. L. Khazov, Nuclear Data Sheets **109**, 517 (2008).

[60] E. Browne and J. Tuli, Nuclear Data Sheets **108**, 2173 (2007).

[61] P. K. Joshi, B. Singh, S. Singh, and A. K. Jain, Nuclear Data Sheets **138**, 1 (2016).

[62] N. Nica, Nuclear Data Sheets **187**, 1 (2023).

[63] E. Browne and J. Tuli, Nuclear Data Sheets **113**, 715 (2012).

[64] E. Browne and J. Tuli, Nuclear Data Sheets **110**, 507 (2009).

[65] B. Singh, Nuclear Data Sheets **102**, 1 (2004).

[66] B. Singh, Nuclear Data Sheets **93**, 33 (2001).

[67] J. Tuli, Nuclear Data Sheets **56**, 607 (1989).

[68] Y. Khazov, A. Rodionov, and G. Shulyak, Nuclear Data Sheets **136**, 163 (2016).

[69] E. Nolte, G. Colombo, S. Z. Gui, G. Ko-

rschinek, W. Schollmeier, P. Kubik, S. Gustavsson, R. Geier, and H. Morinaga, Zeitschrift für Physik A Atoms and Nuclei **306**, 211 (1982).

[70] N. Nica and B. Singh, Nuclear Data Sheets **181**, 1 (2022).

[71] I. Talmi, Nuclear Physics A **172**, 1 (1971).

[72] G. Neyens, Reports on Progress in Physics **66**, 633 (2003).

[73] K. L. Heyde, in *The Nuclear Shell Model: Study Edition* (Springer, 1990) pp. 173–176.

[74] A. de Shalit and M. Goldhaber, Phys. Rev. **92**, 1211 (1953).

[75] I. Talmi, Rev. Mod. Phys. **34**, 704 (1962).

[76] P. Federman and S. Pittel, Physics Letters B **69**, 385 (1977).

[77] H. Watanabe, G. Lorusso, S. Nishimura, T. Otsuka, K. Ogawa, Z. Y. Xu, T. Sumikama, P.-A. Söderström, P. Doornenbal, Z. Li, F. Browne, G. Gey, H. S. Jung, J. Taprogge, Z. Vajta, J. Wu, A. Yagi, H. Baba, G. Benzoni, K. Y. Chae, F. C. L. Crespi, N. Fukuda, R. Gernhäuser, N. Inabe, T. Isobe, A. Jungclaus, D. Kameda, G. D. Kim, Y. K. Kim, I. Kojouharov, F. G. Kondev, T. Kubo, N. Kurz, Y. K. Kwon, G. J. Lane, C.-B. Moon, A. Montaner-Pizá, K. Moschner, F. Naqvi, M. Niikura, H. Nishibata, D. Nishimura, A. Odahara, R. Orlandi, Z. Patel, Z. Podolyák, H. Sakurai, H. Schaffner, G. S. Simpson, K. Steiger, H. Suzuki, H. Takeda, A. Wendt, and K. Yoshinaga, Phys. Rev. Lett. **113**, 042502 (2014).

[78] T. Otsuka, A. Gade, O. Sorlin, T. Suzuki, and Y. Utsuno, Rev. Mod. Phys. **92**, 015002 (2020).

[79] A. K. Jain, B. Maheshwari, and A. Goel, *Nuclear Isomers: A Primer*, 1st ed. (Springer Cham, 2021).

[80] M. Lach, J. Styczen, R. Julin, M. Piiparinen, H. Beuscher, P. Kleinheinz, and J. Blomqvist, Zeitschrift für Physik A Atoms and Nuclei **319**, 235 (1984).

[81] J. J. Valiente-Dobón, P. H. Regan, C. Wheldon, C. Y. Wu, N. Yoshinaga, K. Higashiyama, J. F. Smith, D. Cline, R. S. Chakrawarthy, R. Chapman, M. Cromaz, P. Fallon, S. J. Freeman, A. Görgen, W. Gelletly, A. Hayes, H. Hua, S. D. Langdown, I. Y. Lee, X. Liang, A. O. Macchiavelli, C. J. Pearson, Z. Podolyák, G. Sletten, R. Teng, D. Ward, D. D. Warner, and A. D. Yamamoto, Phys. Rev. C **69**, 024316 (2004).

[82] H. Roth, S. Arnell, D. Foltescu, Ö. Skeppstedt, J. Blomqvist, G. De Angelis, D. Bazzacco, and S. Lunardi, The European Physical Journal A-Hadrons and Nuclei **10**, 275 (2001).

[83] L. Cáceres, M. Górska, A. Jungclaus, M. Pfützner, H. Grawe, F. Nowacki, K. Sieja, S. Pietri, D. Rudolph, Z. Podolyák, P. H. Regan, E. Werner-Malento, P. Detistov, S. Lalkovski, V. Modamio, J. Walker, K. Andgren, P. Bednarczyk, J. Benlliure, G. Benzoni, A. M. Bruce, E. Casarejos, B. Cederwall, F. C. L. Crespi, P. Doornenbal, H. Geissel, J. Gerl, J. Grębosz, B. Hadinia, M. Hellström, R. Hoischen, G. Ilie, A. Khaplanov, M. Kmiecik, I. Kojouharov, R. Kumar, N. Kurz, A. Maj, S. Mandal, F. Montes, G. Martínez-Pinedo, S. Myalski, W. Prokopowicz, H. Schaffner, G. S. Simpson, S. J. Steer, S. Tashenov, O. Wieland, and H. J. Wollersheim, Phys. Rev. C **79**, 011301 (2009).

[84] B. Fogelberg, K. Heyde, and J. Sau, Nuclear Physics A **352**, 157 (1981).

[85] J. Genevey, J. A. Pinston, C. Foin, M. Rejmund, R. F. Casten, H. Faust, and S. Oberstedt, Phys. Rev. C **63**, 054315 (2001).

[86] G. Lo Bianco, P. Paruzzi, K. Schmittgen, R. Reinhardt, A. Gelberg, K. Zell, P. Von Brentano, and N. Blasi, Nuclear Physics A **470**, 266 (1987).

[87] J.-Q. Chen, Nuclear Physics A **626**, 686 (1997).

[88] Z. Y. Xu, Y. Lei, Y. M. Zhao, S. W. Xu, Y. X. Xie, and A. Arima, Phys. Rev. C **79**, 054315 (2009).

[89] G. J. Fu and C. W. Johnson, Physics Letters B **809**, 135705 (2020).

[90] G. J. Fu, C. W. Johnson, P. Van Isacker, and Z. Ren, Phys. Rev. C **103**, L021302 (2021).

[91] Y. M. Zhao and A. Arima, Physics Reports **545**, 1 (2014).

[92] Y. M. Zhao, International Journal of Modern Physics E **34**, 2543001

[93] C. Ma, H. Jiang, Y. Lei, and G. J. Fu, SCIENTIA SINICA Physica, Mechanica & Astronomica **56**, 232001

[94] B. S. Nara Singh, Z. Liu, R. Wadsworth, H. Grawe, T. S. Brock, P. Boutachkov, N. Braun, A. Blazhev, M. Górska, S. Pietri, D. Rudolph, C. Domingo-Pardo, S. J. Steer, A. Ataç, L. Bettermann, L. Cáceres, K. Eppinger, T. Engert, T. Faestermann, F. Farinon, F. Finke, K. Geibel, J. Gerl, R. Gernhäuser, N. Goel, A. Gottardo, J. Grębosz, C. Hinke, R. Hoischen, G. Ilie, H. Iwasaki, J. Jolie, A. Kaşkaş, I. Kojouharov, R. Krücken, N. Kurz, E. Merchán, C. Nociforo, J. Nyberg, M. Pfützner, A. Prochazka, Z. Podolyák, P. H. Regan, P. Reiter, S. Rinta-Antila, C. Scholl, H. Schaffner, P.-A. Söderström, N. Warr, H. Weick, H.-J. Wollersheim, P. J. Woods, F. Nowacki, and K. Sieja, Phys. Rev. Lett. **107**, 172502 (2011).

[95] B. Cederwall, F. G. Moradi, T. Bäck, A. Johnson, J. Blomqvist, E. Clément, G. de France, R. Wadsworth, K. Andgren, K. Lagergren, A. Dijon, G. Jaworski, R. Liotta, C. Qi, B. M. Nyakó, J. Nyberg, M. Palacz, H. Al-Azri, A. Algora, G. de Angelis, A. Ataç, S. Bhattacharyya, T. Brock, J. R. Brown, P. Davies, A. Di Nitto, Z. Dombrádi, A. Gadea, J. Gál, B. Hadinia, F. Johnston-Theasby, P. Joshi, K. Juhász, R. Julin, A. Jungclaus, G. Kalinka, S. O. Kara, A. Khaplanov, J. Kownacki, G. L. Rana, S. M. Lenzi, J. Molnár, R. Moro, D. R. Napoli, B. S. N. Singh, A. Persson, F. Recchia, M. Sandzelius, J.-N. Scheurer, G. Sletten, D. Sohler, P.-A. Söderström, M. J. Taylor, J. Timár, J. J. Valiente-Dobón, E. Vardaci, and S. Williams, Nature **469**, 68 (2011).

[96] C. Qi, J. Blomqvist, T. Bäck, B. Cederwall, A. Johnson, R. J. Liotta, and R. Wyss, Phys. Rev. C **84**, 021301 (2011).

[97] S. Zerguine and P. Van Isacker, Phys. Rev. C **83**, 064314 (2011).

[98] C. Qi, J. Blomqvist, T. Bäck, B. Ceder-

wall, A. Johnson, R. J. Liotta, and R. Wyss, Physica Scripta **2012**, 014031 (2012).

[99] G. J. Fu, J. J. Shen, Y. M. Zhao, and A. Arima, Phys. Rev. C **87**, 044312 (2013).

[100] G. J. Fu, Y. Y. Cheng, Y. M. Zhao, and A. Arima, Phys. Rev. C **94**, 024336 (2016).